Journal of Alloys and Compounds 525 (2012) 143–148

Contents lists available at SciVerse ScienceDirect

Journal of Alloys and Compounds

journal homepage: www.elsevier.com/locate/jallcom

Effect of Ni concentration on electromagnetic wave absorption of (Ni,Mn,Zn)Fe_2O_4/resin particulate composites

Shi-Yuan Tong[a,b], Jenn-Ming Wu[a,*], Mean-Jue Tung[b], Wen-Song Ko[b], Yu-Ting Huang[b], Yen-Ping Wang[b]

[a] Department of Materials Science and Engineering, National Tsing Hua University, Hsinchu 300, Taiwan
[b] Material and Chemical Research Laboratories, Industrial Technology Research Institute, Taiwan

ARTICLE INFO

Article history:
Received 20 December 2011
Received in revised form 8 February 2012
Accepted 13 February 2012
Available online xxx

Keywords:
NiMnZn ferrites
Microwave absorption
Ferrite–resin composites

ABSTRACT

This research aimed to investigate the effect of the Ni-concentration on the modulated crystallographic structure, constitutive electromagnetic properties, and microwave-absorbing behaviors of the MnZn ferrites. Substitution of Ni for Mn induced compressive strains in cubic spinel due to the smaller Ni than Mn. The activation energy of hopping carriers was determined from the plot of resistivity vs temperature. The conduction was considered to be small-polaron hopping among the spinel lattice which was distorted by Ni substitution. The ferrimagnetic properties of $Ni_{0.5x}Mn_{0.5-0.5x}Zn_{0.5}Fe_2O_4$ ferrites were improved with the increasing Ni concentration. The ferrite with $x = 1$ had the lowest intrinsic coercivity ($H_c = 7.4$ Oe) and the highest saturation magnetization ($M_s = 68.9$ emu/g). The increase of the saturation magnetization with the Ni substitution ($x > 0.24$) is ascribed to the dense microstructure with less pores and the decrease of Fe^{2+}/Fe^{3+} ratio. Additionally, a multilayer design of microwave-absorbing structure containing $Ni_{0.5x}Mn_{0.5-0.5x}Zn_{0.5}Fe_2O_4$ granules distributing in a contiguous polymeric matrix was also investigated. The constitutive electromagnetic properties of the composite such as relative permeability and relative permittivity within the whole frequency range were characterized by a combined transmission/reflection method using a coaxial airline fixture. The frequency responses to the electromagnetic field of the ferrite–polymer composites are ascribed to macroscopic magnetic loss and dielectric loss in association with domain-wall oscillation, spin relaxation, and dipolar polarizations. In additions, the microwave-absorbing behaviors of the ferrite–polymer composites were determined using the constitutive electromagnetic properties. The maximum return loss was estimated as −32 dB occurring at 2.3 GHz for 6 mm-thick composite for the composite with $x = 0.24$. For composites with ferrites containing high Ni concentration, the broadening of absorption bandwidth reduced the products of matching thickness and frequency which consequently reduced the required thickness of the microwave absorber. The substitution of Ni for Mn in MnZn ferrites is beneficial in fabricating thin microwave absorbers in GHz frequency range due to the improved electromagnetic lossy characteristics.

1. Introduction

Recently electromagnetic interferences (EMI) which are considered as harmful environmental disturbances have become a serious issue due to the increasing requirement for high data-transferring rates operating within multi-GHz frequency in specific communication equipments such as portable telecommunications, medical equipments, WiMAX/RF identification systems and military radars [1–3]. The undesired electromagnetic interferences generated by the nearby electronic devices operating in GHz frequency may cause error-operation in precision instruments and error-identification in wireless communications. In view of the EMI disturbances, it is necessary to develop microwave absorbers to eliminate electromagnetic wave disturbances in GHz frequency range. Presently, the methodologies to suppress the conduction/radiation EMI noises use absorbing or shielding materials. Absorbing materials can absorb incident microwave energies through electromagnetic loss, while shielding materials reflect microwave energies. To meet requirements, microwave absorbers are designed to have wider absorption band and higher absorption capability [4,5]. To achieve the requirements, electromagnetic lossy granules such as ferrimagnetic ferrite with cubic spinel-type structures are incorporated into polymeric substances to absorb the incident microwave energy. Spinel ferrites provide unique magnetic properties such as high magnetic permeability, high saturation magnetization, and high electrical

* Corresponding author.
E-mail address: wu408410@yahoo.com.tw (J.-M. Wu).

0925-8388/$ – see front matter © 2012 Elsevier B.V. All rights reserved.
doi:10.1016/j.jallcom.2012.02.093

insulations. The high magnetic permeability and high saturation magnetization of ferrites miniaturize the size of the microwave absorber applying in GHz frequency. However, the intrinsic magnetic permeability will drop sharply in the GHz frequency due to magnetic resonance and eddy-current loss, which is known as the phenomenological Snoek limit [6,7]. Fortunately the spinel ferrites possessing high electrical insulation can constrain the circular eddy-currents within the interior sub-grains to maintain the intrinsic permeability essentially unchanged up to the GHz frequency. In additions, the inter-granular polymeric substance distributing around the ferrite granules provides useful advantages of admirable lightweight, reliability and flexibility. There were reviews on homo/hetero microwave absorbing composites comprising magnetic ferrite granules embedded in metallic or insulation mediums, such as Fe_3O_4/Ni-B alloy [8], Fe_3O_4/carbon [9], $NiFe_2O_4$/polystyrene [10] and hexagonal ferrite in paraffin wax [11,12]. Among the ferrites, the MnZn-based ferrite is an outstanding material extensively used as inductor/transformer in power electronics and telecommunication applications. The drawbacks of MnZn ferrite are its low resistivity and low saturation magnetization due to the difficulty in controlling the valence charge of Mn during sintering. Shokrollahi and Janghorban reported that the electrical insulations and condensed microstructures of MnZn ferrites were enhanced by the aids of non-magnetic SiO_2, CaO, and MoO_3 after sintering in mixed N_2/O_2 atmosphere [13]. However, the small additions of above-mentioned oxides in the MnZn ferrite composites cause negative influences on magnetic permeability and saturation magnetizations. Few researches discussed mechanisms of electromagnetic wave absorption of MnZn ferrites with substitution of Ni for Mn. In this work, we substitute Ni for Mn in MnZn ferrites to improve magnetic properties and microwave-absorbing behaviors. A series of the Ni-substituted MnZn ferrites were systematically prepared under the air-sintered profiles. The purpose of magnetic Ni-substitutions in octahedral interstitial sites in the sublattices can stabilize the charge balances of metallic ions in the spinel lattice. The dependence of Ni substitution on the matching frequency/thickness, absorption bandwidth and capability is also investigated.

2. Experimental

Polycrystalline Ni-substituted MnZn ferrites with a stoichiometric formula of $Ni_{0.5x}Mn_{0.5-0.5x}Zn_{0.5}Fe_2O_4$ (where $x = 0$, 0.24, 0.49, 0.75, 1) were synthesized via a standard ceramic processing technique. The ingredients are high purity α-Fe_2O_3, NiO, ZnO and Mn_3O_4 oxides. The mixed powders were milled homogeneously by zirconia medium in distilled water and calcined at 900 °C/2 h to attain spinel phases. The calcined powders were crushed by attrition, sintered at 1200 °C/2 h in air, and then slowly cooled in the furnace. The crystal structures were identified by X-ray diffraction with Cu Kα radiation (XRD, Philips PW1700). The compositions and microstructures were determined by a field emission scanning electron microscopy (FE-SEM, LEO 153). Magnetic hysteresis loops were determined by a vibration sample magnetometer (VSM, Lakeshore 735) with the sweeping fields of 10 kOe. Electrical resistivities were measured by a four-terminal method using a digital electrometer (Keithley, model 2400). The theoretical X-ray density (ρ_x) of ferrite is determined using the formula, $\rho_x = 8\,M/N_v a_t^3$, where M is the molecular weight, N_v is the Avogadro's constant, and a_t is the true value of the lattice parameter. The bulk density (ρ_b) of ferrites is measured by the Archimedes method. The fraction of the inter and intra porosity are estimated using the formula: $(1 - \rho_b/\rho_x) \times 100\%$.

The constitutive electromagnetic properties of ferrite composites have to be taken into consideration because of their ability to attenuate the incident microwave energy. For measuring the constitutive electromagnetic properties, the as-prepared ferrite composites were granulated with a polymeric epoxy resin in a ferrite/resin weight ratio of 90/10 through a dry-mixing method. Epoxy resins with an average particle size of 22–28 μm were supplied from the AkzoNobel manufacturer. The hybridized powders comprising ferrite granules and resin substances were pressed into a torodial shape by a loading pressure of 30 bar and then cured at 160 °C. The torodial specimens were machined to have an outer diameter of 7 mm and an inner diameter of 3.04 mm (thickness 1–2 mm). The *S*-parameters were determined by a bidirectional transmission/reflection method in a coaxial airline fixture with an automatic vector network analyzer (8753D, Agilent, 30 kHz-6 GHz). The constitutive electromagnetic parameters, i.e. relative permeability (μ_r) and permittivity (ε_r), of the composites were extracted by the measured electrical *S*-parameters. The precise method in extracting electromagnetic properties is known as Nicolson–Ross–Weir algorithm [14,15]. The microwave absorbing characteristics, such as return loss and absorption bandwidth, are calculated using the measured electromagnetic properties in a single-layer microwave absorber [16,17]. This method calculates the responses of single-layer absorber terminated by a perfect conductor in a microwave field transmitted under normal incidence. The normalized input impedance (Z) was carried out by computer-aided design programs, utilizing Eq. (1). According to the transmission line theory, the return loss under normal incident microwave is represented by Eq. (2).

$$Z = \sqrt{\frac{\mu_r}{\varepsilon_r}} \tanh\left\{ j\frac{2\pi f t}{c}\sqrt{\mu_r \varepsilon_r} \right\} \quad (1)$$

$$\mathrm{RL}\ (\mathrm{dB}) = 20 \log\left| \frac{Z-1}{Z+1} \right| \quad (2)$$

where Z is the normalized input impedance with respect to the characteristic impedance of free space (377 Ω). The input impedance of incident microwave views from the surface to the terminated conductor through materials; c is the speed of light; μ_r and ε_r are the relative permeability and permittivity; f and t are the frequency of incident wave and the absorber thickness, respectively. The requirements for an ideal microwave absorber are zero-reflecting wave from the absorber interface (i.e. $Z = 1$) and maximum return loss within the finite thickness.

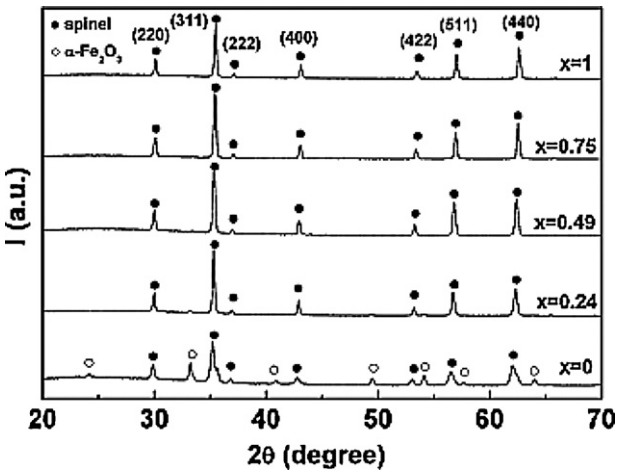

Fig. 1. The XRD patterns of the ferrites with various Ni-concentrations.

3. Results and discussion

The diffraction patterns of ferrites synthesized at 1200 °C are shown in Fig. 1. For the ferrites with $x \geq 0.24$, the corresponding (2 2 0), (3 1 1), (2 2 2), (4 0 0), (4 2 2), (5 1 1) and (4 4 0) peaks are indexed as the cubic spinel with a space group ($fd\bar{3}m$). For the ferrite with $x = 0$, in addition to spinel, the residual hematite phase (α-Fe_2O_3) is observed. The α-Fe_2O_3 phase, being the corundum structure with oxygen ions arranging in a hexagonal close packed framework, is thermodynamically stable at room temperature. When the MnZn ferrite was sintered with sufficient oxygens, the ferrite decomposes reversibly into α-Fe_2O_3, Mn_2O_3 and $ZnFe_2O_4$ phases [18]. It is the reason for the existence of the α-Fe_2O_3 phase. Since no Mn_2O_3 phase is detected, Mn_2O_3 is considered to have reacted with hematites to form spinel ferrites, as indexed in Fig. 1. The observed α-Fe_2O_3 phase is possibly attributed to the Zn evaporation at high temperature. The relative ratio of spinel to hematite is determined by comparing the intensity ratio of the (3 1 1) spinel peak to the (1 0 4) hematite peak [19]. For the ferrite with $x = 0$, the fraction of spinel is estimated as only 65%. With the aid of Ni substitution ($x \geq 0.24$) for Mn, the hematite phase completely disappears. It is attributed to the reaction of divalent Ni ions with the hematite phase to form stable NiMnZn ferrites. The true values (a_t) of the lattice parameters in unit cells of cubic spinel can be estimated by the following Nelson–Riley formula, $F(\theta) = 1/2[(\cos^2\theta/\sin\theta) + (\cos^2\theta/\theta)]$, where θ is the Bragg angle [20]. The a_t value is obtained by extrapolating the straight

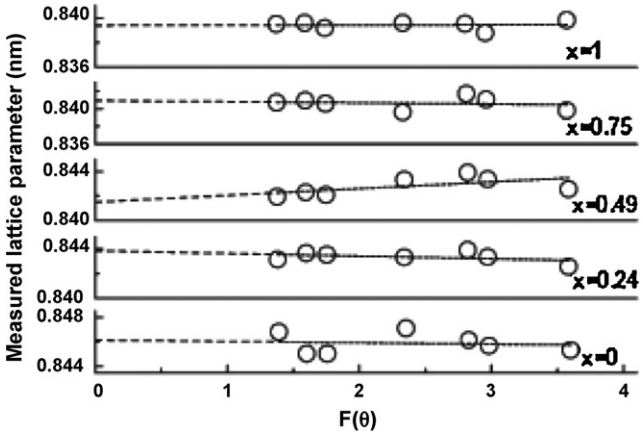

Fig. 2. The dependence of the measured lattice parameters on $F(\theta)$.

Table 1
Lattice parameter (a), X-ray density (ρ_x), bulk density (ρ_b), porosity fraction (PF), polaron radius (γ) and jump distance (L) of ferrite composites.

Ni-content	a_t (nm)	ρ_x (g/cm^3)	ρ_b (g/cm^3)	PF (%)	γ (nm)	L (nm)
$x=0$	0.8462	5.17	4.96	4.05	0.0745	0.2992
$x=0.24$	0.8439	5.22	5.05	3.41	0.0743	0.2984
$x=0.49$	0.8415	5.28	5.09	3.62	0.0741	0.2975
$x=0.75$	0.8410	5.30	5.16	2.72	0.0740	0.2973
$x=1$	0.8394	5.34	5.21	2.49	0.0739	0.2968

line to $F(\theta)=0$, where θ approaches 90°. The measured values of lattice parameters are calculated by the d-spacing of each indexed peak according to the Bragg law. Fig. 2 shows the measured lattice parameters plotting against $F(\theta)$ for ferrites with different Ni concentration. As shown in Table 1, the a_t value of the lattice parameter decreases with increasing Ni concentration. It is due to smaller Ni ions ($R_{Ni^{2+}} = 0.078$ nm) substituting for Mn ions ($R_{Mn^{2+}} = 0.091$ nm) in the spinel lattice. The bulk density and the theoretical density increase significantly with the Ni concentration. On the other hand, the fraction of inter and intra porosity shows decreasing trends. Furthermore, the spinel peaks are observed to move towards lower Bragg angles due to the stress-induced strain in spinel lattices. Fig. 3 shows the dependence of the lattice-induced strain on the Ni concentration. The induced strains are estimated by the following Williamson and Hall equations [21],

$$\frac{\beta\ \cos\theta}{\lambda} = \frac{1}{D} + \frac{\eta\ \sin\theta}{\lambda} \tag{3}$$

where λ is the wavelength of incident X-ray beam, D is the effective crystallization size, η is the lattice-induced strain and β is

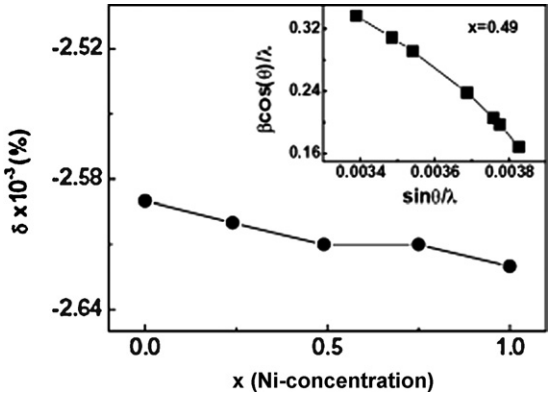

Fig. 3. The variation of lattice strains with the Ni-concentration.

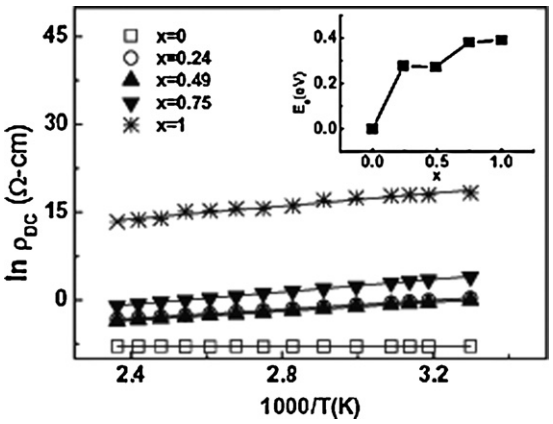

Fig. 4. The variation of DC resistivities with the temperature. Inset shows the activation energy.

the full width at half the maximum intensity. Fig. 3 shows the induced strains in cubic spinel calculating from the slopes in the ($\beta\cos\theta/\lambda$) vs ($\sin\theta/\lambda$) plots. A typical plot ($x=0.49$) is shown in the inset of Fig. 3. It is observed that the substitution of smaller Ni for Mn induces compressive strain. The induced compressive strains in spinel lattices are consistent with the variations of lattice parameters.

In solid ferrites, electron carriers are not completely free. They are usually localized due to strong electron–lattice interaction. Electrons are trapped in potential wells by charge displacements caused by adjacent ions. It is termed as small polarons when the radius of the displacement region is much smaller than the unit-cell dimension. When the spinel lattice is distorted by the Ni substitution, the interaction will affect the radius, jump distance, and jump activation energy of polarons. The polaron radius (γ) of the ferrite is determined by the following equation, $\gamma = (\pi/48N)^{1/3}$, where N is the number of interstitial sites per unit volume ($N = 96/a_t^3$). The jump distance is estimated as $L = (a_t/4)(2)^{1/2}$, where a_t is lattice parameter [22,23]. The polaron radius and jump distances are listed in Table 1. With increasing Ni substitution, the decrease of the polaron radius implies that the localized electron carriers need higher hopping energy to jump in the lattice. In addition, the drift mobility of charge carriers, μ_d, can be expressed as $\mu_d = \mu_0 \exp(D)$, where $\mu_0 = e\nu L^2/kT$ is an constant; e is the electron charge; L is the jump distance; ν is the phonon vibration frequency; k is Boltzmann's constant; T is absolute temperature; $D = -E_a/kT$, where E_a is the activation energy. The $\ln(\mu_d)$ of charge carriers is inversely proportional to the activation energy. Fig. 4 shows the variation of DC resistivity (ρ_{dc}) with temperature (T) (303–423 K) of $Ni_{0.5x}Mn_{0.5-0.5x}Zn_{0.5}Fe_2O_4$ ferrites. The DC resistivity is controlled by the Arrhenius exponential relationship [24]:

$$\rho_{DC} = \rho_0\ \exp\left(\frac{E_a}{kT}\right) \tag{4}$$

where ρ_0 is a constant, E_a is the activation energy in the unit of electron volt (eV). The activation energy is the energy barrier that electrons have to overcome to jump to a neighboring site. As shown in Fig. 4, the DC resistivity decreases with increasing temperature, indicating all ferrites behave as semiconductors. The activation energy of the ferrite increases with the Ni concentration, as shown in the inset of Fig. 4. The ferrite with $x=0$ has the lowest activation energy ($E_a \sim 5\times10^{-5}$ eV) and the highest carrier mobility. Electron carriers hop between Mn^{2+} and Mn^{3+} ions and between Fe^{3+} and Fe^{2+} ions as well. The resistivity increases significantly with the substitution of Ni for Mn. The ferrite with $x=1$ has higher activation energy ($E_a \sim 0.39$ eV) than the other ferrites ($x \le 0.75$). The increase of resistivity with the Ni concentration is partly due to the decrease

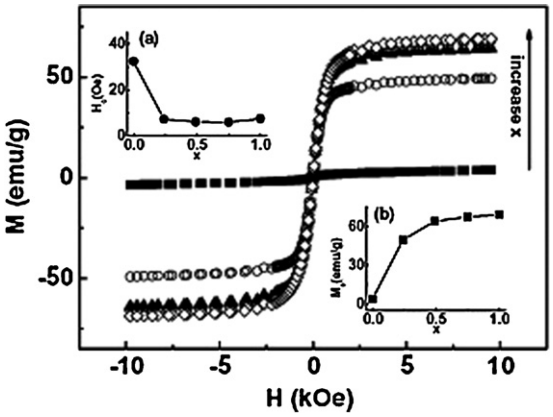

Fig. 5. Magnetic hysteresis loop of ferrite composites with different Ni-substitution. Inset: the variation of (a) intrinsic coercivity and (b) saturation magnetization with the Ni-concentration.

of the Fe^{2+}/Fe^{3+} ratio, and partly due to the increase of activation energy. The increasing activation energy with the Ni concentration is possibly attributed to the induced compressive strain in spinel lattice which increases the electron–lattice interactions.

Fig. 5 shows the magnetic hysteresis loops measured at room temperature. As highlighted in the insets of Fig. 5(a) and (b), the Ni-substituted MnZn ferrites present lower magnetic coercivity (H_c) and higher saturation magnetization (M_s), corresponding with soft ferrimagnetic properties. With increasing Ni concentration, it is observed that the H_c decreases from 32.4 to 7.46 Oe, whereas the M_s increases from 3.68 to 68.9 emu/g. For the ferrite with $x = 0$, the high H_c and the low M_s are due to the presence of the antiferromagnetic hematite phase and the high fraction of inter/intra pores. The hematite phases are antiferromagnetism which possess antiparallel spin-canted configurations and the net magnetizations nearly approach zero. The hematite phases as well as inter/intra pores cause a domain-wall pinning and a magnetic decoupling between grains. It results in high H_c. For ferrites with $x \geq 0.24$, the hematite phase disappear and the fraction of inter and intra pores decreases, causing the decrease of H_c. The disappearance of the hematite phase is evidenced by XRD. The saturation magnetization of ferrites strongly depends on the magnetic-spin ordering structure associated with the site preference of the metal ions and the crystal-field stabilization in the spinel lattice. The spinel lattice has two interstitial sublattices surrounded by oxygen ions, i.e. tetrahedral A-sites and octahedral B-sites. The magnetic spins on these two sublattices are antiparallel coupled via the superexchange interactions. The total magnetic moments are determined by the difference of the magnetic spin moments in A and B sublattice ($M = |M_A - M_B|$). For the ferrite with $x = 0$, the lowest M_s value is mainly attributed to the presence of the antiferromagnetic hematite and the high fractions of inter/intra pores. For the ferrite with $x = 0.24$, the significant increase of the saturation magnetization is due to the complete reaction of Ni with the hematite phase, resulting in a stable NiMnZn ferrite without any residual phase. As for ferrites with $x > 0.24$, the slight increase of M_s with the Ni-substitution is partly attributed to the denser microstructure as well as the decreasing magnetic coercivity, and partly attributed to the decrease of the Fe^{2+}/Fe^{3+} ratio. The replacement of Ni for Mn stabilizes the charge balance of metallic ions which results in the decrease of the Fe^{2+}/Fe^{3+} ratio, which is supported by the resistivity data. Each Fe^{2+} ion possesses 4 unpaired electrons while each Fe^{3+} ion possesses 5 unpaired electrons. Hence, the saturation magnetization increases slightly with the Ni concentration for $x > 0.24$.

Fig. 6 illustrates the frequency dependences of the relative permeability and the relative permittivity of the ferrite–resin composites. As shown in Fig. 6(a) and (b), the real part (μ') and imaginary part (μ'') of permeability of the composite containing the ferrite with $x = 0$ remain nearly constant and substantially independent with frequency. For the ferrite–resin composites containing ferrites with $x \geq 0.24$, the μ' increases to about 10–12 at 100 MHz and the μ' decreases abruptly with increasing frequency. The decrease of μ' value with increasing frequency is due to magnetic resonance and eddy-current loss. The dissipation of microwave energies by the composites is evidenced in the μ''–f dependence. The μ''–f dependence shows a broad maximal peak at around 0.8 GHz. Ferrite composites absorb microwave energies through domain wall oscillations and spin exchange interactions, which are characterized as the combinatorial magnetic resonances of Debye-relaxations [25]. The eddy current loss induced by alternating electromagnetic fields in the composites causes the decrease of the μ' in the high frequency range. Ferrites with high electrical resistivity can suppress the eddy current loss in the composites and maintain the μ' to be essentially unchanged till a higher frequency. The imaginary part of the permeability induced by magnetic resonances is expressed using the M_s and H_a terms, as shown in the formula of $\mu'' = M_s/3\mu_0 H_a \alpha$, where μ_0 is the permeability of free space, H_a is magnetocrystalline anisotropy field, and α is Gilbert's damping factor. In general, the magnetocrystalline anisotropy of ferrites is proportional to the magnetic coercivity. The decrease of H_c and the increase of M_s result in the higher imaginary part of permeability for the composites containing ferrites with $x \geq 0.24$.

Fig. 6(c) and (d) shows that the frequency dependences of the real part (ε') and the imaginary part (ε'') of permittivity. The variation of the relative permittivity with frequency resembles to the μ'–f dependence. For the composite containing the ferrite with $x = 0$, the ε' is smaller and remains nearly constant with frequency due to the residual non-polar hematite and polymeric substances [26]. For the composites containing ferrites with $x \geq 0.24$, the ε' remain nearly constant of about 10–15 around 100 MHz and then decrease abruptly with frequency till about 1 GHz. Dipolar interfacial polarizations usually occur in polycrystalline ferrites when space charges accumulate at grain/grain boundaries. The decrease of the ε' with the frequency is attributed to the Maxwell–Wagner interfacial polarization, which is in agreement with the Koop's phenomenological theory [27,28]. The ε'' reaches a maximum at around 150 MHz and then decreases with increasing frequency, which is in accordance with the theory of the Maxwell–Wagner interfacial polarization.

The variation of the attenuation factor (α) with the Ni concentration is shown in Fig. 7. The attenuation factor (dB/cm) is determined as follows [29]:

$$\alpha = \frac{\pi}{\lambda}[2(\mu''\varepsilon'' - \mu'\varepsilon') + 4\sqrt{(\varepsilon'\mu')^2 + (\varepsilon'\mu'')^2 + (\varepsilon''\mu')^2 + (\varepsilon''\mu'')^2}]^{0.5} \quad (5)$$

where λ is the electromagnetic wavelength. The α value increases monotonously with frequency. The α value of the composite containing the ferrite with $x = 0$ is lower than those of the composites containing ferrites with $x \geq 0.24$. It is consistent with the measured imaginary part of permeability and permittivity spectra. The substitution of Ni for Mn in MnZn ferrites improves the microwave absorption.

The ability to absorb microwave energy of the composites depends on their relative permeability and permittivity spectra. To further illustrate the microwave absorption properties, the return losses of single-layer absorbing composites terminating with a back conductor are calculated using Eqs. (1) and (2). A return loss of −10 dB is equivalent to 90% of microwave energy dissipating by the microwave

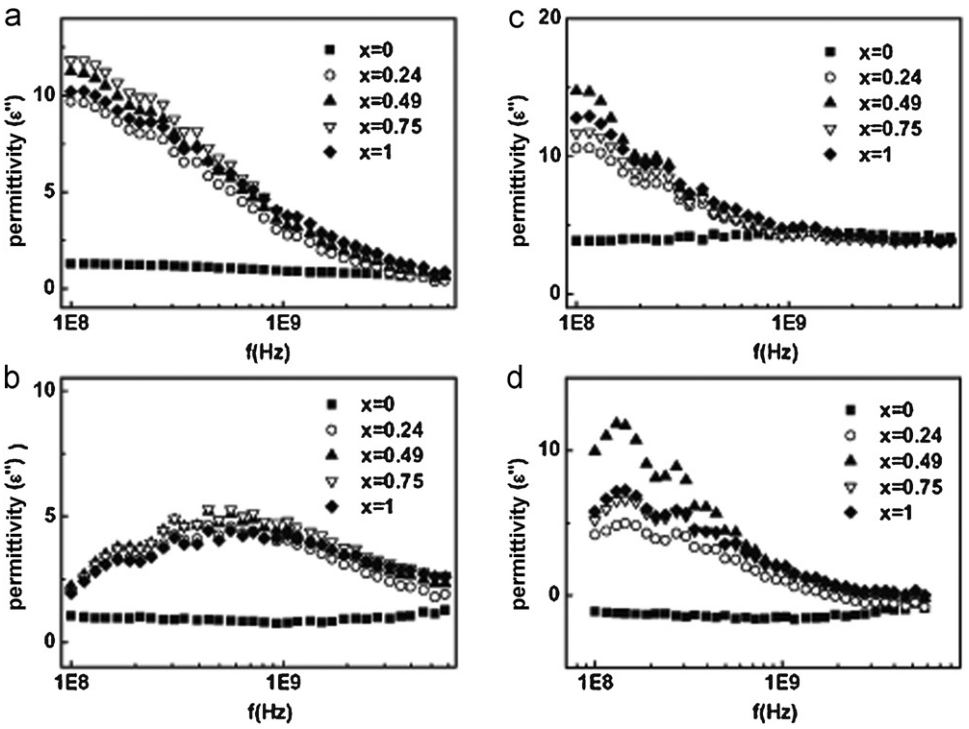

Fig. 6. Electromagnetic characterization: the variation of (a) the real part of permeability, (b) the imaginary part of permeability, (c) the real part of permittivity, and (d) the imaginary part of permittivity with the Ni-concentration.

absorber under normal incidence. The absorption bandwidth corresponds to the upper/lower frequency range of a return loss of −10 dB. The calculated return losses of ferrite composites with a 6 mm thickness are shown in Fig. 8. When the Ni concentration of the ferrites in the composites increases, the minimum dip of the return loss moves toward lower frequency and the absorption bandwidth at −10 dB (ΔB) increases. The return loss of the heterogeneous ferrite–resin composite containing the ferrite with $x = 0.24$ and a 6 mm thickness is estimated as −32 dB at 2.3 GHz. The high return loss of the ferrite composite with $x = 0.24$ was attributed to the lowest value of $(Z-1)/(Z+1)$ term which denoted the nearly perfect wave-impedance matching viewing from the surface through absorbers to the terminated conductor.

Fig. 9(a) shows the variations of return loss with the absorber thickness for ferrites with different Ni-concentration. The return losses of the ferrite composites ($x = 0.24$–1) decreased with the thickness of the absorber, while that of the ferrite composite ($x = 0$) had a minimum dip. The matching conditions for ferrite composites occurred at the maximal return loss. The return loss for the composite of $x = 0.24$ with a 6 mm thickness was −32 dB in the matching condition at 2.3 GHz. Fig. 9(b) shows the variation of the absorption bandwidth with the Ni concentration and the absorber thickness. It is clear that the absorption bandwidth (ΔB) increases slightly with the increase of the Ni concentration and with the decrease of the absorber thickness. Lee reported the return loss and the absorption bandwidth of the MnZn ferrite–polymer composites with a 5 mm thickness were −26 dB and 3 GHz, respectively [30]. In comparison with their work, the return loss and the absorption bandwidth of the composites ($x = 0.24$) with a 6 mm thickness increased to −30 dB and 3.6 GHz, respectively, by substituting Ni for Mn in MnZn ferrites. The enhanced microwave-absorbing properties, i.e. the higher return loss and wider absorption bandwidth, were due to increased permeability and permittivity of the ferrites after Ni

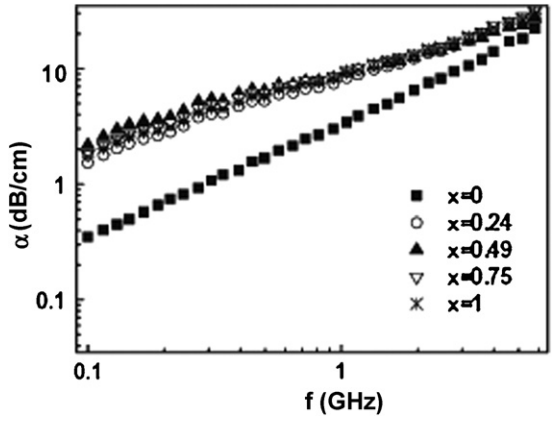

Fig. 7. The calculated attenuation coefficients for ferrites with different Ni-substitution.

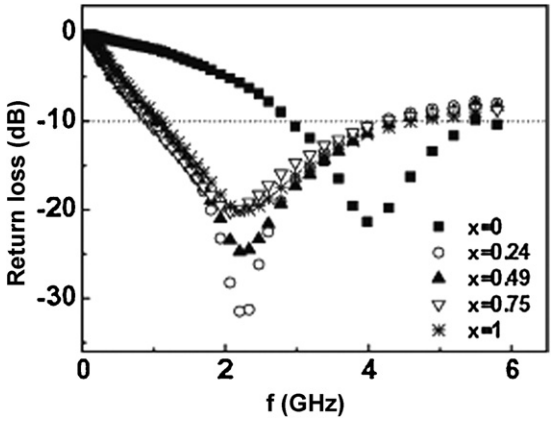

Fig. 8. The calculated return loss of 6 mm-thick composites with different Ni-substitution.

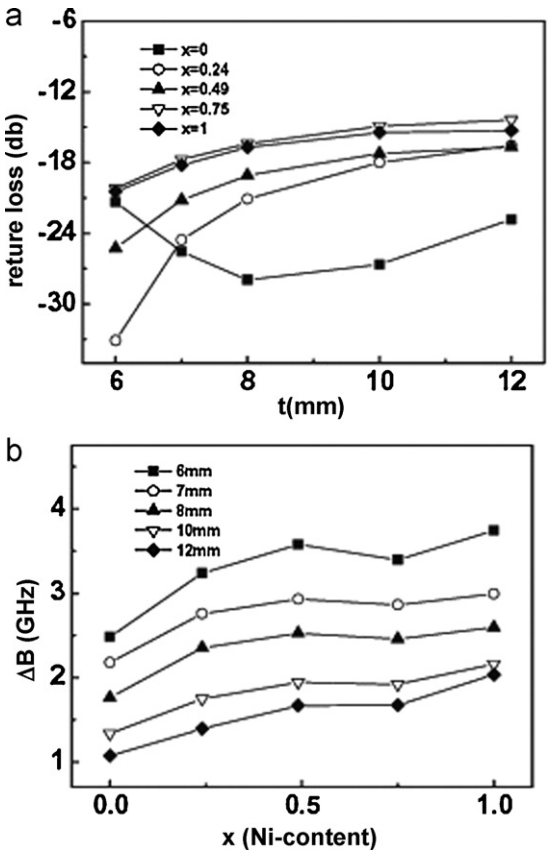

Fig. 9. (a) The variations of return loss on absorber thickness with different Ni-concentrations, (b) the calculated absorption bandwidth at −10 dB as a function of the Ni-substitution with various thickness.

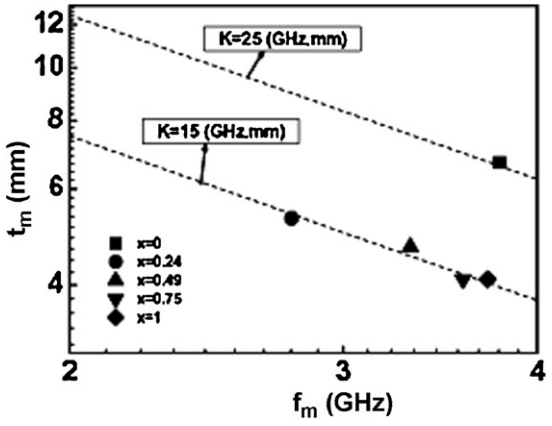

Fig. 10. Relationship between matching frequency and matching thickness for ferrites with different Ni-substitution.

substitution for Mn in MnZn ferrites. In additions, the matching thickness (t_m) and the matching frequency (f_m) of the microwave absorbers are inversely proportion to μ''. The matching conditions can be estimated by the formula, $c = 2\pi K\mu''$, where $K = f_m t_m$ and c is the velocity of light [31]. In the ferrite composites, the higher μ'' value results in the smaller K value. The K value is adopted as an index to design microwave absorbers. The smaller K value denotes that the microwave absorbers should be designed to have a thinner matching thickness or a lower matching frequency. Fig. 10 shows the matching frequency plotted against the matching thickness for the ferrite–resin composite absorbers. The dashed line denotes the K value. The K value for the composites containing ferrites with $x \geq 0.24$ is smaller than that for the composite containing a ferrite with $x = 0$. It represents that thinner microwave absorbers can be used at a specific matching frequency if ferrite–resin composites employ Ni to substitute for Mn in the MnZn ferrites.

4. Conclusion

The Ni-substituted MnZn ferrites were prepared by a standard ceramic process under air-sintered atmospheres. The Ni-substituted MnZn ferrites ($x \geq 0.24$) have soft ferrimagnetic behavior with lower H_c and higher M_s due to the absence of the antiferromagnetic hematite and the less inter and intra pores. With increasing substitution of Ni for Mn, the activation energy of the small-polaron defects increases, while the polaron radius and jump distance decrease. The return loss of heterogeneous ferrite–resin composites with 6 mm thickness is estimated as −32 dB at 2.3 GHz for $x = 0.24$. By increasing the Ni substitution for Mn in ferrites, the ferrite–resin composite has a wider bandwidth and a higher potential to be designed as a microwave absorber in the GHz range with a thinner thickness.

Acknowledgment

The authors gratefully acknowledge the MCL/ITRI for support through Project No. A354DA1320.

References

[1] E. Hanada, Y. Antoku, S. Tani, M. Kimura, A. Hasegawa, S. Urano, K. Ohe, M. Yamaki, Y. Nose, IEEE Trans. Electromagn. Compat. 42 (2000) 470–476.
[2] L. Yang, A. Rida, R. Vyas, M.M. Tentzeris, IEEE Trans. Microw. Theory Technol. 55 (2007) 2894–2901.
[3] M. Cao, R. Qin, C. Qiu, J. Zhu, Mater. Des. 24 (2003) 391–396.
[4] L. Yan, J. Wang, Y. Ye, Z. Hao, Q. Liu, F. Li, J. Alloys Compd. 487 (2009) 708–711.
[5] M.J. Park, J. Choi, S.S. Kim, IEEE Trans. Magn. 36 (2000) 3272–3274.
[6] J.L. Snoek, Physica 14 (1948) 207–217.
[7] G.G. Bush, Physica 63 (1988) 3765–3767.
[8] X. Li, X. Han, Y. Tan, P. Xu, J. Alloys Compd. 464 (2008) 352–356.
[9] S. Ni, X. Wang, G. Zhou, F. Yang, J. Wang, D. He, J. Alloys Compd. 489 (2010) 252–256.
[10] H. Zhao, X. Sun, C. Mao, J. Du, Physica B 404 (2009) 69–72.
[11] J. Xu, H. Zou, H. Li, G. Li, S. Gan, G. Hong, J. Alloys Compd. 490 (2010) 552–556.
[12] N. Chen, K. Yang, M. Gu, J. Alloys Compd. 490 (2010) 609–612.
[13] H. Shokrollahi, K. Janghorban, Mater. Sci. Eng. B 141 (2007) 91–97.
[14] A.M. Nicolson, G. Ross, IEEE Trans. Instrum. Meas. 19 (6) (1970) 377–382.
[15] J.J. Baker, E.J. Vanzura, W.A. Kissick, IEEE Trans. Microw. Theory Technol. 38 (8) (1990) 1096–1103.
[16] H.M. Musal, D.C. Smith, IEEE Trans. Magn. 26 (1990) 1462–1464.
[17] T. Giannakopoulou, A. Kontogeorgakos, G. Kordas, J. Magn. Magn. Mater. 263 (2003) 173–181.
[18] M. Rozman, M. Drofenik, J. Am. Ceram. Soc. 81 (1998) 1757–1764.
[19] B.D. Cullity, Elements of X-Ray Diffraction, 1977, Chapter 14, pp. 397–419.
[20] J.B. Nelson, D.P. Riley, Proc. Phys. Soc. 57 (1945) 160–167.
[21] K. Williamson, W.H. Hall, Acta Metall. 1 (1953) 22–31.
[22] A.J. Bosman, J.H. Van Dall, Adv. Phys. 19 (1970) 1–7.
[23] B. Gillot, F. Jemmali, Phys. Status Solidi A 76 (1983) 601–608.
[24] A.I.E. Shora, M.A.E. Hiti, M.K.E. Nimr, M.A. Ahmed, A.M.E Hasab, J. Magn. Magn. Mater. 204 (1999) 20–28.
[25] T. Tsutaoka, J. Appl. Phys. 93 (2003) 2789–2796.
[26] J.C. Papaioannou, G.S. Patermarakis, H.S. Karayianni, J. Phys. Chem. Solids 66 (2005) 839–844.
[27] M.R. Anantharaman, S. Sindhu, S. Jagatheesan, K.A. Malini, P. Kurian, J. Phys. D: Appl. Phys. 32 (1999) 1801–1810.
[28] C.G. Koops, Phys. Rev. 83 (1951) 121–124.
[29] A.R. Bueno, M.L. Gregori, M.C.S. Nobrega, J. Magn. Magn. Mater. 320 (2008) 864–870.
[30] B.T. Lee, H.C. Kim, Jpn. J. Appl. Phys. 35 (1996) 3401–3406.
[31] T. Maeda, S. Sugimoto, T. Kagotani, N. Tezuka, K. Inomata, J. Magn. Magn. Mater. 281 (2004) 195–205.